Laser surface modifications of Fe-14Cr ferritic alloy for improved corrosion performance

Ali Hemmasian Ettefagh, Hao Wen, Ardalan Chaichi, Md Imdadul Islam, Fengyuan Lu, Manas Gartia, Shengmin Guo

PII: S0257-8972(19)31184-3

DOI: https://doi.org/10.1016/j.surfcoat.2019.125194

Reference: SCT 125194

To appear in: *Surface & Coatings Technology*

Received date: 28 September 2019

Revised date: 6 November 2019

Accepted date: 23 November 2019

Please cite this article as: A.H. Ettefagh, H. Wen, A. Chaichi, et al., Laser surface modifications of Fe-14Cr ferritic alloy for improved corrosion performance, *Surface & Coatings Technology* (2018), https://doi.org/10.1016/j.surfcoat.2019.125194

Laser Surface Modifications of Fe-14Cr Ferritic Alloy for Improved Corrosion Performance

Ali Hemmasian Ettefagh[1], Hao Wen, Ardalan Chaichi, Md Imdadul Islam, Fengyuan Lu, Manas Gartia, Shengmin Guo

Department of Mechanical and Industrial Engineering, Louisiana State University, 70803, Baton Rouge, LA, USA

Abstract: Laser processing parameters of an ytterbium fiber laser were explored using a two-stage searching strategy to form an optimum surface layer on Fe-14Cr ferritic alloy samples for improved corrosion performance. With one or two passes of laser surface scanning, corrosion behavior and surface layer uniformity were investigated for different laser parameters utilizing energy-dispersive x-ray spectroscopy (EDS) and electrochemical tests in saltwater. The optimum laser processing parameters were found to be 175 w of laser power, 200 mm/s of scanning speed, and 0.025 mm of hatching space. Corrosion behavior of laser-treated samples with the optimum laser parameters was found to be 5 and 13 times better respectively than the baseline sample in 3.5 wt% NaCl water solution, in term of corrosion rate. The formation of a uniform thin oxidation layer was the main reason for the improved corrosion performance.

Keywords: Laser; Surface Modification; Ferritic Alloy; Corrosion; Surface Scanning; Protective Coating

1. Introduction

Since the first introduction of Oxide Dispersion Strengthened (ODS) alloys several decades ago, ODS alloys have found applications in many industrial sections [1-3]. To disperse nano-

[1] - corresponding author: ahemma3@lsu.edu

sized oxide particles into the alloy matrix, various fabrication methods can be used, including selective laser melting [4], mechanical alloying (MA) [5, 6], sol-immersion methods [7], and internal oxidation [8]. Among these techniques, MA, coupled with hot isostatic pressing (HIP) or hot extrusion based consolidation process [9, 10], is the most widely used method to produce bulk ODS alloys. Spark plasma sintering (SPS) is a comparatively new technique which has been utilized recently for the consolidation of powder mixtures. In this method, rapid consolidation takes place under a very high heating rate with pulsed electrical current. The rapid process will not only maintain the basic properties/microstructures of the initial powders, but also improve the mechanical properties of the consolidated parts [11]. Recently, SPS has been successfully applied to consolidate ODS steels [9, 12]. Typically, low voltage (<10 V) but high current (1000–5000 A) DC pulses are applied to alloy powders contained in a graphite mold, along with a uniaxial pressure (up to 100 MPa). After reaching the target temperature, the sample is typically held isothermally for 3 to 20 min; and then followed by rapid cooling [13].

Fe-14Cr ODS steel is a potential candidate for applications such as nuclear reactors, combustion parts for engines, and stirrers for the glass industry due to its unique properties at elevated temperatures and supercritical environments [14, 15]. Due to the moderate Cr content, the corrosion resistance of Fe-14Cr ODS is worse than high Cr content steels. Coatings are typically applied to improve the corrosion resistance [2, 14] of steels.

Thanks to the distinguished properties of laser beams, such as high intensity and little divergence, laser surface modification has gained increasing interests in recent years. Laser based surface modifications can be applied to improve wear behaviors, biocompatibility, and corrosion performance [16-20]. Common laser based alloy surface treatment techniques include laser alloying, laser cladding, laser peening, laser hardening, and surface laser scanning [20-27],

among others. In this paper, the optimization of laser surface treatment on Fe-14Cr samples was performed, with the goal of improving the corrosion resistance of Fe-14Cr ODS steel. To speed up the laser optimization process, a two-stage searching process was adopted to effectively identify the optimum laser processing parameters, which can lead to the formation of a uniform surface oxide coating on Fe-14Cr ferritic alloy. Laser source parameters including laser power, scanning speed, and hatching space were manipulated to produce the most uniform protective layer on the alloy surface. In the first stage, the optimized laser energy density was identified; and in the second stage, the optimization of the laser power/speed combinations was performed. Optimum values were obtained based on the uniformity of the formed surface scale and corrosion behavior of the processed surfaces. Applying two best sets of these parameters, two samples were treated with a single pass of laser scanning and two others were treated with an additional pass of laser scan, with laser scanning tracks at 90 degrees of angle to the first layer of scan. The corrosion properties of these laser processed samples were compared with the sample without surface treatment. The protective nature of the formed surface layer was characterized using Raman spectroscopy and X-Ray diffraction (XRD) techniques.

2. Materials and methods

Fe-14Cr-2W-0.3Ti-0.3Y_2O_3 (wt.%) powder mixture was prepared using commercial pure powders of Fe, Cr, W, Ti and Y_2O_3 purchased from a commercial source (>99.9 wt.%, Alfa Aesar). Mechanical alloying was performed on the powder mixture for 10 hours in a high energy ball mill (SPEXSamplePrep Mixer/Mill) with a stainless-steel ball to powder ratio of 10:1 under an argon environment. A typical SEM image of the powders and the size distribution after 10

hours of ball milling measured by laser diffraction spectrometry (Malvern MASTERSIZER 3000) can be seen in Figure 1.

Consolidation of Fe-14Cr-2W-0.3Ti-0.3Y_2O_3 powders was conducted using a Spark Plasma Sintering (SPS) system (FUJI-SPS DR. SINTER LAB) with a ϕ15mm graphite die at an axial pressure of 45 MPa. During the SPS process, the temperature was raised from room temperature to 700 °C at a rate of 100 °C/min, and then to 850 °C at a rate of 50 °C/min. The samples were kept at 850 °C for 4 minutes before cooled down to room temperature. Afterward, surface treatment was applied on the Fe-14Cr-2W-0.3Ti-0.3Y_2O_3 SPS samples using a custom laser system composing a 200W IPG ytterbium fiber laser and a laser scan head (ProSeries II). A 58 μm laser spot size was achieved using a JENar F-Theta lens at the focal plane which was 403.8 mm below the lens surface. The test was performed in an inert argon environment by vacuum the chamber from the initial atmosphere pressure to 150 Pascal and then refill the chamber with argon gas back to the atmosphere pressure. The residual oxygen in the chamber is one of the sources of oxygen for the formation of oxides. It is well known that the protective nature of an oxide layer highly depends on the oxygen partial pressure. Simply using air can lead to the formation of a non-protective layer on the alloy surface [28]. In addition, for a working condition with relatively high vapor pressure, the oxide layer is less protective due to the loss of Cr through $CrO_2(OH)_2$ evaporation [29, 30]. To provide a suitable condition for forming a protective layer, the tests were performed in a controlled atmosphere with an oxygen concentration about 0.03%. The laser was in continuous wave mode and the wavelength is 1064 nm. Figure 2 demonstrates a schematic design of the custom laser system [31, 32] and the used scanning pattern to achieve full surface coverage of the disk shaped samples with a diameter of 15 mm.

For laser processing, surface energy density (E') is calculated with the unit of J/mm^2 as a fraction with the numerator of laser power (P in W) over the product of laser scanning speed (v in mm/s) and hatching space (H in mm) as the denominator. To evaluate the impact of laser surface modifications of Fe-14Cr-2W-0.3Ti-0.3Y_2O_3 SPS samples with respect to the corrosion performance, polarization curves were obtained by sweeping the potential in the range of -1 V_{SCE} to -0.2 V_{SCE} at a rate of 1.67 mV/s. The tests were conducted using a CHI 604C electrochemical workstation in 3.5 wt% NaCl water solution with the exposed surface area of 0.7 cm^2. With a standard three-electrode corrosion cell setup, the sample acts as the working electrode; a platinum wire acts as the counter electrode, and a saturated calomel electrode (SCE) acts as the reference. The tests were performed at room temperature with naturally dissolved oxygen. The surface of the samples was polished before the tests with sandpapers (grit size 320-1000) and immersed freely in the solution to attain a stable value of open circuit potential (OCP) for 30 min. Each sample was subjected to electrochemical measurement at least three times for high reproducibility. Elemental distribution of each sample was performed with EDS (EDAX Pegasus EDS) and Raman spectroscopy (Renishaw inVia Reflex Raman Microscope) was conducted on the laser modified samples to identify the formed oxide layer. For Raman mapping, a 532 nm laser was used with magnification of 100X and step size of 500 nm. Phase evaluation was performed using CuKα radiation with 0.039 degrees as the scan step size and with a 2θ range of 20-70° by a PANalytical Empyrean XRD at ambient temperature. The surface micro-hardness was measured using a Vickers microhardness tester (FM-110, Future-tech corp., Tokyo, Japan).

3. Results and discussion

3.1. Towards laser parameter optimization

Laser processing parameters include laser power (P), scanning speed (v), and hatching space (H). In this paper, the criterion for laser parameter optimization is to achieve a uniform surface coating, with the hypothesis that a uniform surface coating should lead to an improved corrosion performance. To optimize the laser parameters, a two-stage process is adopted with stage-one for identifying the suitable laser energy level while stage-two for identifying the best laser power-scanning speed combination.

For stage-one, the attempted three sets of laser parameters and the calculated energy density (E') can be found in Table 1. In these sets, laser power and scanning speed were kept constant while hatching space was altered for three different energy densities (samples Y01, Y02 and Y03). Besides, to evaluate the role of the laser scanning process, one sample was prepared without laser scanning process and was tagged SPS. Visual inspection reveals a high surface roughness on the Y03 sample, which indicates excess laser power density. And in case of Y01, a visible stripe surface pattern suggests an uneven molten track coverage on the surface. Figure 3 (a) demonstrates the polarization test results of samples with the stage-one laser processing parameters together with the results of SPS sample. Based on these curves, corrosion current density (i_{corr}) and corrosion potential (E_{corr}) were calculated by Tafel extrapolation method and the results are shown in Table 2. It can be seen that Y02 exhibits the best corrosion performance by offering the lowest corrosion current density and the most positive corrosion potential. In addition, all three laser treated samples show a better corrosion performance compared to the SPS sample. It has been argued that the formation of the surface layer containing chromium, titanium, and yttrium oxides protects the surface and improves the corrosion resistance of samples [33]. To check the uniformity of surface coatings, elemental distributions on the surface of Y01 to Y03 samples were performed by EDS. The results of these measurements are

presented in Figure 3 (b). From these maps, it is clear that iron is concentrated in regions with low levels of chromium, yttrium, and titanium. In other words, the later three elements seem to form regions that cover the iron base but these iron-depleted regions are not uniform over the entire sample surfaces. From the measurements, it is obvious that the formed layers on Y01 and Y03 are not uniform, with the molten track marks clearly shown. For case Y02, the non-uniformity has decreased in some levels qualitatively. On the other hand, unlike surface treated samples, the map for SPS sample shows a uniform distribution of all elements confirming the uniform chemical composition of samples after ball milling. Based on visual inspection and the results of corrosion test and elemental distribution, the energy density of Y02 was judged the best.

For stage-two, the energy density of Y02 was selected and fixed while three different laser power/speed combinations, Y04-Y06 in Table 3, were evaluated. To establish the link between surface coating uniformity and the corrosion performance, corrosion tests and elemental distribution were performed on Y04 to Y06 samples. The results of these tests can be seen in Figure 4 and Table 4 along with the previous results for Y02 and SPS samples. From the elemental map, it is clear that Y06 exhibits the best uniformity. The same deduction can be extracted from corrosion results and the trend of the corrosion rates is more or less proportional to the uniformity of the surface layer. In addition, the corrosion rate of SPS sample is the worst compared to any of the laser-treated samples. Based on the obtained results from all the 6 sets, Y02 and Y06 laser parameters were identified to be the best ones.

3.2. Laser double scan and corrosion performance

To further improve the coating surface uniformity, Y02 and Y06 laser parameters were selected for an additional surface scan with 90 degrees of angle to the first pass of laser scanning.

The samples with double passes of laser processing are named YY02 and YY06. To demonstrate the effectiveness of the additional pass of laser scanning, polarization curves and surface elemental distributions were obtained for these samples, Figure 5, and the associated corrosion parameters are summarized in Table 5. After applying two passes of surface laser scanning, the corrosion performance improved even more, suggesting the formation of a more protective layer on the surface. According to Table 5, the corrosion rate of YY06 sample has been decreased about 13 times compared to the same sample without any surface laser scanning. This value for Y06 with a single pass of laser scanning is almost 5 times, indicating the role of laser scanning in forming the protective layer. Besides, according to Figure 5 (b), the elemental distribution of Cr, Y and Ti elements have been improved after two passes of surface treatment, suggesting a uniform layer on the surface, possibly consist of oxides of the mentioned elements.

3.3. Coating characterizations

To understand the mechanisms for improved corrosion performance, additional surface characterizations including X-ray diffraction, Raman spectroscopy, and microhardness were performed on the samples. Figure 6 (a) shows the XRD patterns of SPS, Y02, Y06, YY02, and YY06 samples. After laser surface processing, the formation of Cr_2O_3 is apparent, with a relatively high intensity for the relevant XRD peaks. Small amounts of other oxides such as $Y_2Ti_2O_7$ and Fe_2CrO_4 are also detected on the laser processed samples, which are all known to be protective oxides. Main detected peaks in SPS sample are associated with chiefly iron and chromium elements which were applied to make this alloy. These peaks are much less pronounced in Y02 and Y06 samples and completely disappeared after two passes of laser scanning on YY02 and YY06 samples. Dominant peaks of chromium oxide in laser-scanned samples prove that by providing enough energy, Cr_2O_3 will form on the top layer of the laser

processed samples. Although the chamber was purged with Argon before the laser processing, residual oxygen is still expected in the laser processing chamber. Y06 and YY06 samples were recognized for the uniform elemental distributions and good corrosion performance. Figure 6 (b) and (c) show the cross-sectional Raman maps of Y06 and YY06 samples. The green color illustrates the formation of a primary Cr_2O_3 layer on the surface, which is mostly responsible for the improvement of corrosion behavior. Pink color shows the substrate right beneath the Cr_2O_3 coating. As can be seen, the thickness of the Cr_2O_3 coating increases from □3 μm to □5 μm after performing the second pass of laser treatment.

The results of XRD and Raman spectroscopy can justify the noted improvement of corrosion resistance in Y06 and YY06 samples. XRD results of the laser-scanned samples confirm the elemental map presented in Figure 5 (b), which imply that the major elements on the surface of Y2, Y6, YY02, and YY06 are Cr, Y, and Ti. XRD results proof that the formed phases are mainly Cr_2O_3 (confirmed by Raman spectroscopy) and a tiny amount of $Y_2Ti_2O_7$ (Figure 6). These results endorse the corrosion trend of the modified samples presented in Figure 5 (a). The development of Cr_2O_3 is well-known to be the protection mechanism of chromium contained steels and expected to improve the corrosion performance of Fe-14Cr. The formation of Cr_2O_3 and a tiny amount of Fe_2CrO_4 in laser processed samples suggests that due to the high temperature during the laser melting process, a uniform oxide layer can be formed under optimized laser processing parameters. The formation of a titanium-yttrium oxide in the shape of Y-Ti-O nanoclusters [34] or $Y_2Ti_2O_7$ and/or Y_2TiO_5 [6] is claimed to be the consequence of adding Y_2O_3 to the initial powder mixture during the mechanical milling step. Besides, it has been stated that despite the protective role of chromium oxide scale on the surface, the stability of small yttrium oxide particles results in finer grains of the matrix and finer grains enhance the

diffusion of Cr to the surface and accelerate the formation of protective layer along with providing oxygen [35, 36]. Thus, optimized laser surface treatment provided a proper situation for the formation of protective oxides on the surface of Fe-14Cr-2W-0.3Ti-0.3Y_2O_3 alloy. In contrast, the SPS process, with a relatively low processing temperature, cannot provide the suitable condition for the formation of a uniform protective layer. Higher corrosion rate of SPS sample is the outcome of lacking a protective layer on the surface.

The results of microhardness tests on the selected samples along with the error bar (one-standard-deviation measure of the data scatter) are presented in Figure 7. As can be seen, the hardness of the SPS sample (without any surface laser processing) is the minimum one. After one pass of surface laser treatment, the hardness value dramatically increases due to the formation of the mentioned oxide phases on the surface layer along with the microstructural changes of the substrate. To quantify laser surface treatment, two parameters are commonly considered, which are 1. Laser interaction time (laser spot size divided by the scanning speed), and 2. Beam density (laser power divided by the spot size). Laser interaction time is 0.322 ms and 0.290 ms for Y02 and Y06 respectively, and the beam density is $4.73x10^4$ W/mm^2 and $6.62x10^4$ W/mm^2 for Y02 and Y06 respectively. It is well known that by increasing these laser parameters, the average surface hardness would increase [37]. In Y02 and Y06 cases, the combination of laser interaction time and beam density values made the almost equal surface hardness results understandable. The microhardness values for YY02 and YY06 samples are slightly higher than the values for the Y02 and Y06 samples, indicating a slightly thickened coating layer, in agreement with Figure 6 results. More detailed assessment on hardness results will be reflected in future publications.

4. Conclusions

The optimum laser processing parameters were obtained in a two-stage searching process for improved corrosion performance of Fe-14Cr ferritic alloy. Laser parameters including laser power, scanning speed, and hatching space were manipulated to produce a uniform protective layer on the alloy surface.

- The two-stage searching strategy, where the laser energy density was optimized first, followed by the optimization of the laser power/speed combinations, was an effective method to optimize laser processing parameters.
- Improved corrosion performance and the uniformity of elemental map distribution lead to the identification of two sets of optimized laser processing parameters. The best sample was scanned using a laser power of 175 W, a scanning speed of 200 mm, and a hatching space of 0.025 mm. The corrosion resistance of the laser processed sample was 5 times higher in a simulated marine condition than the bare sample due to the formation of the protective coatings on the surface.
- A second pass of laser scanning with 90 degrees of angle to the first layer of laser scan decreased the corrosion rate by almost 90% compared to the bare sample.
- The formation of Cr_2O_3 on the surface was identified with Raman Spectroscopy as well as XRD and can be recognized as the main reason for the improved corrosion performance of laser-scanned samples.

5. Acknowledgment

This research project is sponsored by the NSF EPSCoR CIMM project under award #OIA-1541079 and Louisiana Board of Regents. Raman experiments were performed at LSU's Shared

Instrumentation Facility (SIF). Ardalan Chaichi is supported by LSU Economic Development Assistantships (EDA).

References

[1] C.-L. Chen, Study of W-Co ODS coating on stainless steels by mechanical alloying, Surface Coatings Technology 350 (2018) 954-961.

[2] C. Kim, S.H. Kim, J.-H. Cha, C. Jang, T.K. Kim, Cr diffusion coating to improve the corrosion resistance of an ODS steel in super-critical carbon dioxide environment, Surface Coatings Technology (2019).

[3] Z. Oksiuta, P. Hosemann, S. Vogel, N. Baluc, Microstructure examination of Fe–14Cr ODS ferritic steels produced through different processing routes, Journal of Nuclear Materials 451(1-3) (2014) 320-327.

[4] J.C. Walker, K.M. Berggreen, A.R. Jones, C.J. Sutcliffe, Fabrication of Fe–Cr–Al oxide dispersion strengthened PM2000 alloy using selective laser melting, Advanced Engineering Materials 11(7) (2009) 541-546.

[5] C.-L. Chen, Investigation of W-Ti ODS coating on SUS304 steel fabricated by mechanical alloying technique, Surface Coatings Technology 350 (2018) 1105-1111.

[6] T. Liu, C. Wang, H. Shen, Y. Cao, W. Chou, Influence of YH2 nanoparticles addition on the microstructure and mechanical properties of oxide dispersion strengthened ferritic alloys, Advanced Engineering Materials 17(5) (2015) 689-696.

[7] L. Guo, C. Jia, B. Hu, H. Li, Microstructure and mechanical properties of an oxide dispersion strengthened ferritic steel by a new fabrication route, Materials Science Engineering: A 527(20) (2010) 5220-5224.

[8] J.H. Schneibel, S. Shim, Nano-scale oxide dispersoids by internal oxidation of Fe–Ti–Y intermetallics, Materials Science Engineering: A 488(1-2) (2008) 134-138.

[9] M. Frelek-Kozak, L. Kurpaska, E. Wyszkowska, J. Jagielski, W. Pawlak, I. Jozwik, M. Chmielewski, K. Perkowski, M. Lewandowska, Influence of consolidation process on functional properties of steels, Surface Coatings Technology 355 (2018) 234-239.

[10] V. De Castro, E. Marquis, S. Lozano-Perez, R. Pareja, M. Jenkins, Stability of nanoscale secondary phases in an oxide dispersion strengthened Fe–12Cr alloy, Acta Materialia 59(10) (2011) 3927-3936.

[11] M. Suárez, A. Fernández, J. Menéndez, R. Torrecillas, H. Kessel, J. Hennicke, R. Kirchner, T. Kessel, Challenges and opportunities for spark plasma sintering: a key technology for a new generation of materials, Sintering Applications, IntechOpen2013.

[12] Z. Li, Z. Lu, R. Xie, C. Lu, C. Liu, Effect of spark plasma sintering temperature on microstructure and mechanical properties of 14Cr-ODS ferritic steels, Materials Science Engineering: A 660 (2016) 52-60.

[13] M.A. Auger, Y. Huang, H. Zhang, C. Jones, Z. Hong, M. Moody, S.G. Roberts, P.S. Grant, Microstructural and mechanical characterisation of Fe-14Cr-0.22 Hf alloy fabricated by spark plasma sintering, Journal of Alloys Compounds 762 (2018) 678-687.

[14] X. Li, H. Chu, Y. Chen, P. Hua, G. Wang, W. Kong, J. Chen, Y. Wu, W. Zhou, Microstructure and properties of the laser cladding ODS layers on CLAM steel, Surface Coatings Technology 357 (2019) 172-179.

[15] E. Vasquez, P.-F. Giroux, F. Lomello, A. Chniouel, H. Maskrot, F. Schuster, P. Castany, Elaboration of oxide dispersion strengthened Fe-14Cr stainless steel by selective laser melting, Journal of Materials Processing Technology 267 (2019) 403-413.

[16] C. Park, A. Sim, S. Ahn, H. Kang, E.-J. Chun, Influence of laser surface engineering of AISI P20-improved mold steel on wear and corrosion behaviors, Surface Coatings Technology (2019).

[17] S.M. Asl, M. Ganjali, M. Karimi, Surface modification of 316L stainless steel by laser-treated HA-PLA nanocomposite films toward enhanced biocompatibility and corrosion-resistance in vitro, Surface Coatings Technology 363 (2019) 236-243.

[18] A. Hemmasian Ettefagh, C. Zeng, S. Guo, J. Raush, Corrosion behavior of additively manufactured Ti-6Al-4V parts and the effect of post annealing, Additive Manufacturing 28 (2019) 252-258.

[19] A. Hemmasian Ettefagh, S. Guo, Electrochemical behavior of AISI316L stainless steel parts produced by laser-based powder bed fusion process and the effect of post annealing process, Additive Manufacturing 22 (2018) 153-156.

[20] M. Moradi, D. Ghorbani, M.K. Moghadam, M. Kazazi, F. Rouzbahani, S. Karazi, Nd: YAG laser hardening of AISI 410 stainless steel: Microstructural evaluation, mechanical properties, and corrosion behavior, Journal of Alloys & Compounds 795 (2019) 213-222.

[21] J.D. Majumdar, I. Manna, Mechanical properties of a laser-surface-alloyed magnesium-based alloy (AZ91) with nickel, Scripta Materialia 62(8) (2010) 579-581.

[22] P. Volovitch, J. Masse, A. Fabre, L. Barrallier, W. Saikaly, Microstructure and corrosion resistance of magnesium alloy ZE41 with laser surface cladding by Al–Si powder, Surface Coatings Technology 202(20) (2008) 4901-4914.

[23] C. Ma, G. Peng, L. Nie, H. Liu, Y. Guan, Laser surface modification of Mg-Gd-Ca alloy for corrosion resistance and biocompatibility enhancement, Applied Surface Science 445 (2018) 211-216.

[24] L. Ardila-Rodríguez, B. Menezes, L. Pereira, R. Takahashi, A. Oliveira, D. Travessa, Surface modification of aluminum alloys with carbon nanotubes by laser surface melting, Surface Coatings Technology (2019) 124930.

[25] H. Abedi, M. Salehi, M. Yazdkhasti, A. Hemmasian Ettefagh, Effect of high temperature post-oxidizing on tribological and corrosion behavior of plasma nitrided AISI 316 austenitic stainless steel, Vacuum 85(3) (2010) 443-447.

[26] M. Moradi, H. Arabi, S.J. Nasab, K.Y. Benyounis, A comparative study of laser surface hardening of AISI 410 and 420 martensitic stainless steels by using diode laser, Optics & Laser Technology 111 (2019) 347-357.

[27] M. Moradi, M.K. Moghadam, M. Kazazi, Improved laser surface hardening of AISI 4130 low alloy steel with electrophoretically deposited carbon coating, Optik 178 (2019) 614-622.

[28] D. Baer, Protective and non-protective oxide formation on 304 stainless steel, Applications of surface science 7(1-2) (1981) 69-82.

[29] F. Liu, J.E. Tang, T. Jonsson, S. Canovic, K. Segerdahl, J.-E. Svensson, M. Halvarsson, Microstructural investigation of protective and non-protective oxides on 11% chromium steel, J Oxidation of Metals 66(5-6) (2006) 295-319.

[30] H. Asteman, J.-E. Svensson, L.-G. Johansson, Oxidation of 310 steel in H2O/O2 mixtures at 600 C: the effect of water-vapour-enhanced chromium evaporation, Corrosion Science 44(11) (2002) 2635-2649.

[31] H. Wen, C. Zeng, A. Hemmasian Ettefagh, J. Gao, S. Guo, Laser surface treatment of Ti-10Mo alloy under Ar and N2 environment for biomedical application, Journal of Laser Applications 31(2) (2019) 022012.

[32] A. Hemmasian Ettefagh, H. Wen, F. Lu, S. Guo, Phase Evolution and Corrosion Performance of Laser Processed Oxide Dispersion Strengthened Ferritic Alloys, ASME 2018 International Mechanical Engineering Congress and Exposition, American Society of Mechanical Engineers Digital Collection, 2019.

[33] H. Cho, A. Kimura, Corrosion resistance of high-Cr oxide dispersion strengthened ferritic steels in super-critical pressurized water, Journal of Nuclear Materials 367 (2007) 1180-1184.

[34] C. Lu, Z. Lu, R. Xie, Z. Li, C. Liu, L. Wang, Effect of Y/Ti atomic ratio on microstructure of oxide dispersion strengthened alloys, Materials Characterization 134 (2017) 35-40.

[35] H. Hu, Z. Zhou, L. Liao, L. Zhang, M. Wang, S. Li, C. Ge, Corrosion behavior of a 14Cr-ODS steel in supercritical water, Journal of Nuclear Materials 437(1-3) (2013) 196-200.

[36] D. Hoelzer, B. Pint, I. Wright, A microstructural study of the oxide scale formation on ODS Fe–13Cr steel, Journal of Nuclear Materials 283 (2000) 1306-1310.

[37] M. Moradi, M. KaramiMoghadam, High power diode laser surface hardening of AISI 4130; statistical modelling and optimization, Optics & Laser Technology 111 (2019) 554-570.

Table 1- Identify the best laser energy density.

Sample No.	Laser Power P (W)	Scanning Speed v (mm/s)	Hatching Space H (mm)	Energy Density E' (J/mm^2)
SPS	N/A	N/A	N/A	N/A
Y01	125	180	0.080	8.68
Y02	125	180	0.020	34.72
Y03	125	180	0.012	57.87

Table 2- Corrosion potential and current density obtained from Tafel curves in Figure 3 (a).

Sample No.	E_{corr} (v)	i_{corr} ($\mu A/cm^2$)
SPS	-0.728	97.7
Y01	-0.615	72.4
Y02	-0.557	25.7
Y03	-0.581	33.9

Table 3- Identify the best laser power-speed combinations.

Sample No.	Laser Power P (W)	Scanning Speed v (mm/s)	Hatching Space H (mm)	Energy Density E' (J/mm^2)
SPS	N/A	N/A	N/A	N/A
Y02	125	180	0.020	34.72
Y04	44	50	0.025	35.20
Y05	75	86	0.025	34.89
Y06	175	200	0.025	35.00

Table 4- Corrosion potential and current density obtained from Tafel curves in Figure 4 (a).

Sample No.	E_{corr} (v)	i_{corr} (µA/cm2)
SPS	-0.728	97.7
Y02	-0.557	25.7
Y04	-0.612	71.1
Y05	-0.592	58.9
Y06	-0.526	18.2

Table 5- Corrosion potential and current density obtained from Tafel curves in Figure 5 (a).

Sample No.	E_{corr} (v)	i_{corr} ($\mu A/cm^2$)
SPS	-0.728	97.7
Y02	-0.557	25.7
Y06	-0.526	18.2
YY02	-0.469	11.7
YY06	-0.427	7.4

Figure 1- (a) Powder size distribution after 10 hours of ball milling, (b) SEM micrograph of Fe-14Cr-2W-0.3Ti-0.3Y2O3 powders.

Figure 2- (a) Schematic drawing of the custom laser system used for surface laser processing [31, 32], (b) Laser pattern used for scanning the surface of the samples.

Figure 1- (a) Polarization curves in 3.5% NaCl Solution, and (b) Elemental map for Fe, Cr, Y, and Ti using EDS on SEM for samples Y01 to Y03 along with the SPS sample. The scale bars are all indicating 100 µm.

Figure 2- (a) Polarization curves in 3.5% NaCl Solution, and (b) Elemental map for Fe, Cr, Y and Ti using EDS on SEM for samples Y04 to Y06. The scale bars are all indicating 100 µm.

Figure 3- (a) Polarization curves in 3.5% NaCl Solution, and (b) Elemental map for Fe, Cr, Y and Ti using EDS on SEM for optimum sets of parameters with single or double passes of surface treatment. The scale bars are all indicating 100 µm.

Figure 4- (a) XRD plots of SPS only and Laser surface treated samples of Fe-14Cr alloy, (b) Cross-sectional Raman spectroscopy and microscopy of Y06, (c) Cross-sectional Raman spectroscopy and microscopy of YY06.

Figure 5- Micro-hardness measurements for the 3-SPS sample (without surface scanning), Y02 and Y06 with one round of surface laser scanning and YY02 and YY06 with two passes of laser surface treatment.

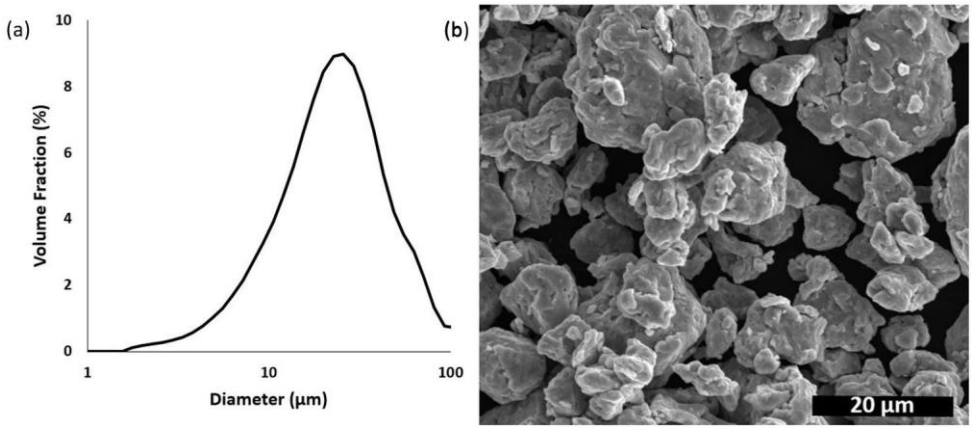

Figure 6

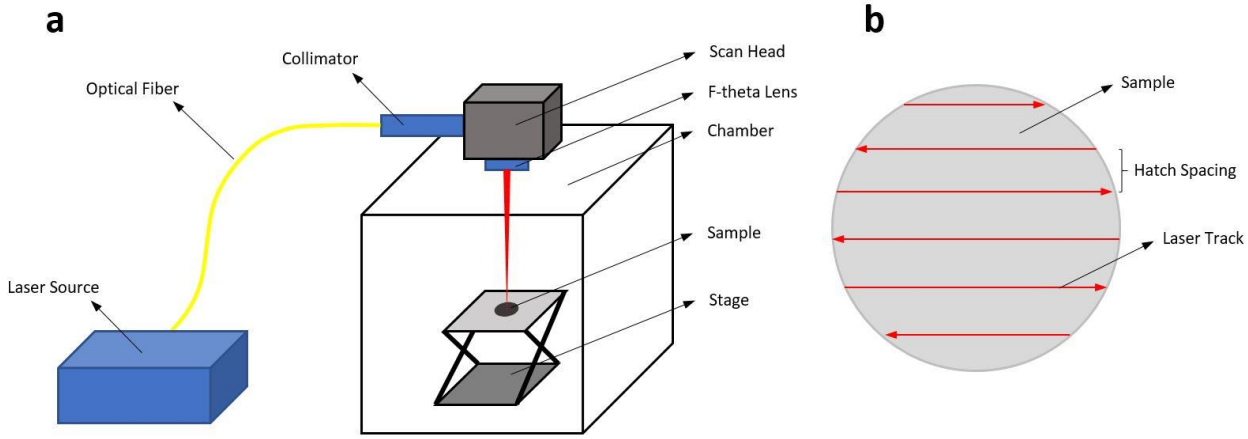

Figure 7

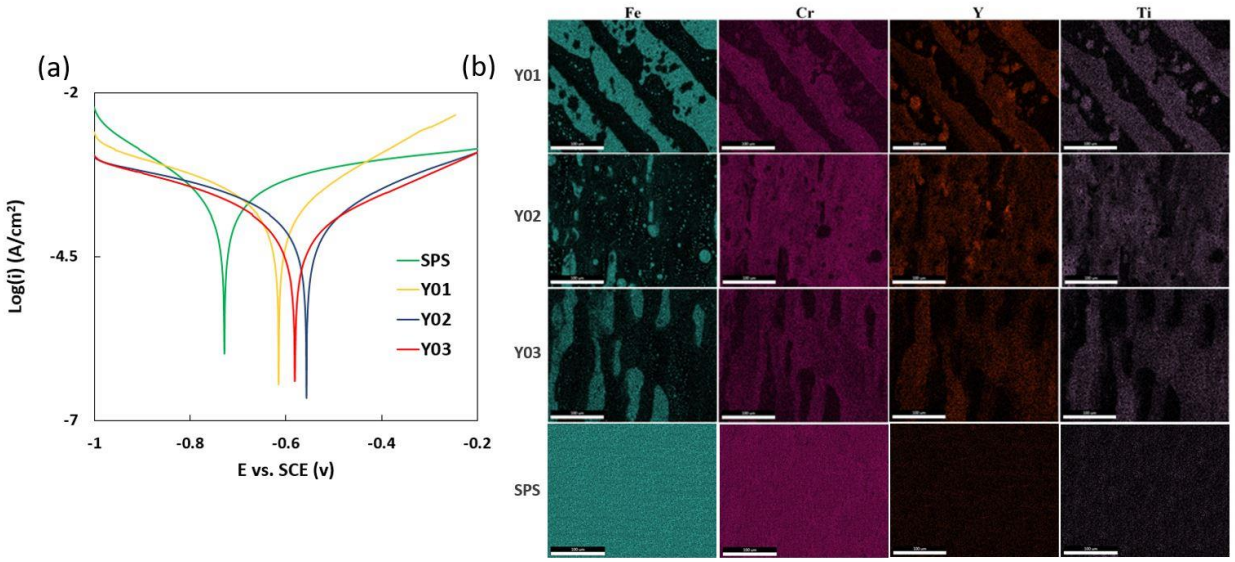

Figure 8

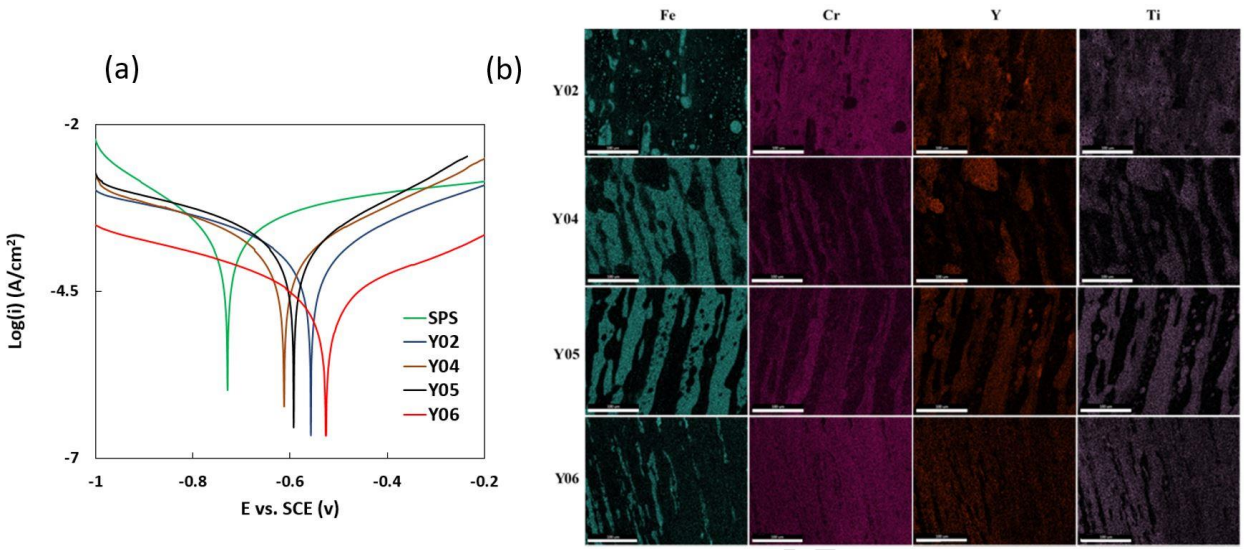

Figure 9

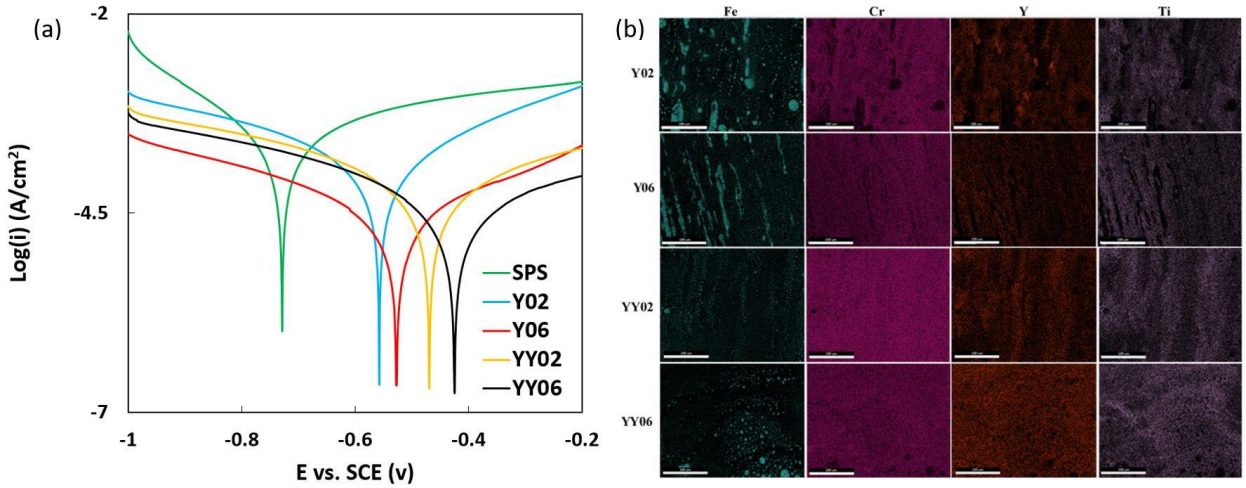

Figure 10

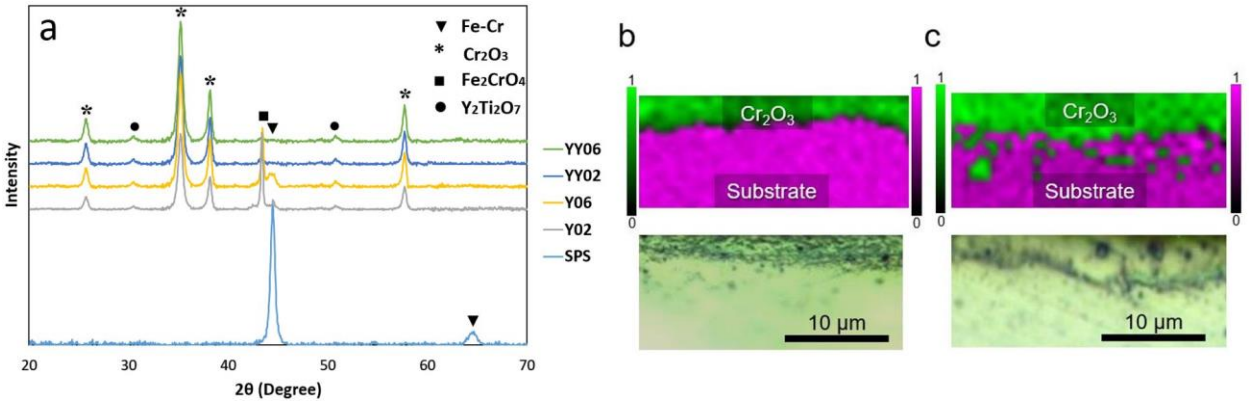

Figure 11

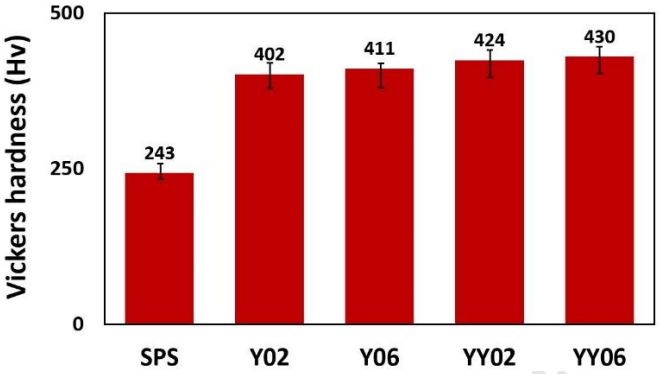

Figure 12

Graphical abstract

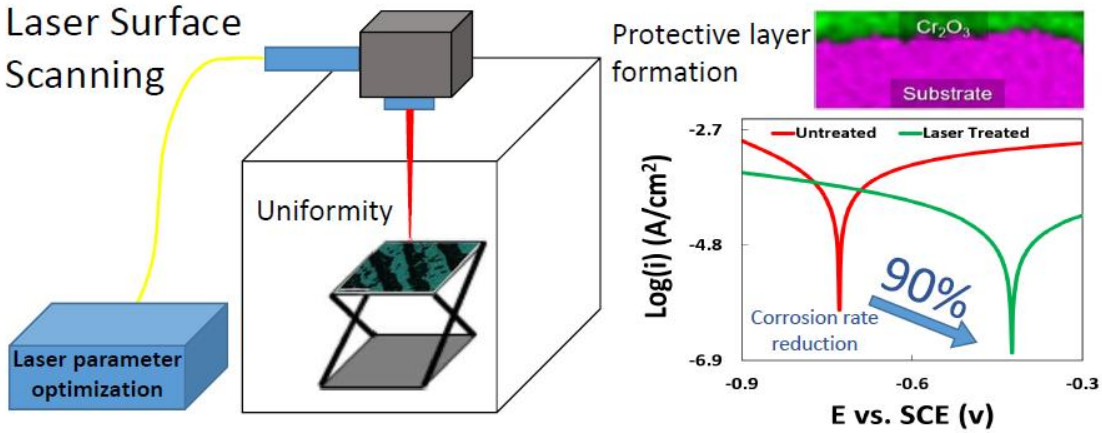

Highlights

- The optimum laser processing parameters were obtained for the formation of a uniform surface oxide coating on Fe-14Cr ferritic alloy for improved corrosion performance.
- Laser parameters including laser power, scanning speed, and hatching space were manipulated to produce the most uniform protective layer on the alloy surface.
- For the optimized set, high quality protective layers were formed on the surfaces, which decreased the corrosion rate by almost 90% compared to the bare sample.